Manuscript accepted in the Int J of Refractory Metals and Hard Materials

Incipient plasticity in tungsten during nanoindentation: dependence on surface roughness, probe radius and crystal orientation

Ben D. Beake[1*] and Saurav Goel[2]

[1] Micro Materials Ltd., Willow House, Yale Business Village,Ellice Way, Wrexham, LL13 7YL, UK

[2] School of Aerospace, Transport and Manufacturing, Cranfield University, Bedford, MK43 0AL, UK

* Corresponding author. Email: ben@micromaterials.co.uk; Tel: +44 1978 261615.

Abstract

The influence of crystallographic orientation, contact size and surface roughness effects on incipient plasticity in tungsten were investigated by nanoindentation with indenters with a range of end radius (150, 350, 720 and 2800 nm) in single crystal samples with the (100) and (111) orientations. Results for the single crystals were compared to those for a reference polycrystalline tungsten sample tested under the same conditions. Surface roughness measurements showed that the R_a surface roughness was around 2, 4, and 6 nm for the (100), (111) and polycrystalline samples respectively. A strong size effect was observed, with the stress for incipient plasticity increasing as the indenter radius decreased. The maximum shear stress approached the theoretical shear strength when W(100) was indented using the tip with the smallest radius. The higher roughness and greater dislocation density on the W(111) and polycrystalline samples contributed to yield occurring at lower stresses.

Keywords: tungsten; anisotropy; nanoindentation; incipient plasticity

Abbreviations:

BCC	Body centred cubic
FCC	Face centred cubic
ISE	Indentation size effect
NPL	National Physical Laboratory
RMS	Root mean square

Nomenclature:

a	Contact radius
Al	Aluminium
E or E_s	Elastic modulus of the material
E_r	Reduced elastic modulus
h^*	Characteristic length
h_c	Contact depth
h_{max}	Depth under maximum load at pop-in
h_r	Residual indentation depth
H_0	Macroscopic hardness
L	Applied load
G	Shear modulus
Mo	Molybdenum
P_m	Mean contact pressure
p_0	Maximum contact pressure
R	End radius of the indenter
R_a	Average surface roughness
Ta	Tantalum
W	Tungsten
τ_{max}	Maximum shear stress

1. Introduction

Tungsten (W) is a technologically important BCC metal with potential applications in the next generation of nuclear reactors, being a favoured choice for plasma-facing components in fusion reactors [1-3]. ISO:14577 specifies that W being very close to elastically isotropic (Zener anisotropy ratio is 1.01) while having a high elastic modulus makes it an important reference material for indirectly calibrating nanomechanical test instruments due to its high sensitivity to the instrument frame stiffness. It has the highest melting point of all the metals and its high temperature nanomechanical behaviour is beginning to be explored [4]. However, as yet relatively little attention has been given to the influence of crystallographic orientation, loading rate and surface roughness, and how these might influence size effects in incipient plasticity and hardness at the nano-/ and micro/-scale [5].

During nanoindentation, both BCC and FCC metals can show displacement bursts that are known as “pop-ins” [6-8]. Typically in BCC metals such as W, Cr, Mo and Ta, a single yield event is observed while for close packed metals multiple pop-in (“staircase”) behaviour is more common

[9]. It is generally accepted that with a sharp indenter, incipient plasticity at the pop-in event occurs due to homologous dislocation nucleation and the shear stress required can approach the theoretical strength [10]. The presence of thick thermally grown oxide layers can modify the stress distributions under the indenter so that a pop-in may be associated with oxide fracture [6]. However, as the native oxide on tungsten is much thinner, of the order of ~0.7 nm thick at room temperature [11], oxide fracture is not thought to contribute to the observed behaviour [12]. Shim et al. [13] noted that the increase in strength as the size of the contact decreases can be considered to be a different type of indentation size effect to that commonly seen in hardness, since the latter depends on the yielding and work-hardening behaviour of the material and the former on the stress to initiate dislocation plasticity. In a fusion reactor, tungsten is subjected to intense bombardment from alpha particles and hydrogen ions which can cause indentation size effects[14]. Being able to deconvolute the origins of the different indentation size effects (ISEs) on the observed behaviour is essential since they will all contribute to the behaviour at a similar scale (e.g. within ~100 nm of the surface).

Yao et al. [1] reported a dependence on crystallographic orientation on electrochemically polished, vacuum annealed (12h at 950 ºC) and D-implanted single crystal tungsten with the critical load for pop-in with a R = 675 nm indenter being much larger on (100) and (110) surfaces than on the (111) orientation. Contrarily, they found no orientation dependence for hardness. Stelmashenkoet al. [15] reported Vickers hardness measurements showing higher hardness and higher pile-up around the indentations for W(100). Pethica's group noted that after mechanical polishing a number of dislocation systems are active at low load in W(100) and a clear single pop-in was not observed [16]. They also reported that the hardness of mechanically polished W samples determined at depths higher than the pop-in event was higher than that of electropolished samples.

Most studies on incipient plasticity of pure metals have used indenters of one or at most two radii, making the effect of tip radius difficult to establish accurately. There have been two recent reports using a wide range of tip radius. Shim et al. [13] studied the influence of indenter radius (R = 0.58 to 209 microns) on pop-in occurring in the FCC metal Ni(100) and reported that the critical

loads and maximum shear stresses under the indenter increased as the radius decreased. Wu et al. [17] investigated the onset of plasticity in the BCC metal chromium using indenters with tip radius ranging from 60-759 nm and also found that the stress required for incipient plasticity increased with a reduction in tip radius.

There has been recent interest in the influence of the surface state on the load required for pop-in [8, 9, 12, 14]. Although it is generally accepted that pop-in events require highly polished surfaces, it is a common practice in the literature for either the surface roughness to notbe quoted or for only an approximate measure of R_a to be provided. On Al(001), Shibutani et al. [8] observed that the critical load scaled inversely with surface roughness. A reduction in R_a from ~2.5 nm to under 0.5 nm resulted in the critical load increasing by a factor of 3. Bahr et al. [6] reported that, as opposed to electropolished surfaces, mechanically polished W single crystals did not show pop-ins. Biener et al [9] reported that on Ta(001) there was no difference between electropolished or mechanically polished surfaces provided a high-quality surface finish was obtained. They found a tight distribution in the critical load for pop-in for a Ta(001) surface with the RMS roughness well below 1 nm. Introducing surface roughness on Ta by low-energy Ar^+ ion bombardment suppressed the linear elastic regime and the pop-in behaviour.

This work reports novel findings obtained from nanoindentation experiments performed on tungsten samples. The objective of this study was to investigate the contribution of size effects to incipient plasticity in tungsten using a wide range of indenter radius (0.15-2.8 microns). Alongside this, the influence of crystallographic orientation, loading rate and surface roughness were also studied on single crystals of tungsten with the (100) and (111) orientation and a reference polycrystalline tungsten sample. Nanoindentation data at a lower load were supplemented by measurements to 500 mN to determine the conventional indentation size effect in hardness.

2. Experimental

2.1 Materials

Two high purity polished tungsten single crystals and a high purity polycrystalline tungsten certified reference sample were tested. The sample with (100) orientation was provided by KRISS (Korea), originally for the VAMAS TWA22 Intercomparison on nanoindentation, being supplied by Goodfellow (USA) and polished by KRISS. The sample with (111) orientation was supplied by Goodfellow (UK) and was of thickness 2 mm and diameter 6 mm, and was polished on one side to better than 1 micron (W 002166). The quoted elastic modulus and Poisson's ratio of the samples were 411 GPa and 0.28 respectively. The polycrystalline certified reference tungsten sample ("JGA-105", Instrumented Indentation Reference Block, DataSure-IIT, NPL, Teddington, UK) was obtained from NPL, based in the UK. Its elastic modulus and Poisson's ratio were determined by NPL in accordance with BS EN 843-2:2006. The certified value of E obtained by NPL was 411.5 ± 1.9 GPa and the Poisson's ratio was 0.2806 ± 0.0017. The density of the polycrystalline sample was 1.9259 g cm^{-3}. The sample was coarse-grained with an average grain size in the region of 10 μm. The tungsten samples were tested as-received and no further attempt was made to modify surface roughness or near-surface defect density by further polishing or annealing steps. Surface roughness was measured over a line profile using the Surface Topography option in the Scanning Module of the NanoTest using (i) a spheroconical diamond probe with a nominal end radius of 5 microns (the actual end radius was separately determined as 4 microns) (ii) a well-worn Berkovich indenter with an end radius of 1 μm. Surface roughness of the single crystal samples was also measured at the 5 μm x 5 μm scale by AFM (NanoSurf Nanite B). Table 1 summarises the surface roughness data. The AFM images revealed the presence of very fine polishing marks on the surface of the (111) oriented W which were absent on the (100) oriented W.

Table 1.Surface Roughness of the measured samples

	R_a surface roughness (nm)		
	AFM (5 μm x 5 μm area)	Line scan with R = 1.0 μm diamond (over 10 μm length)	Line scan with R = 4.0 μm diamond (over 10 μm length)
W(100)	1.4 ± 0.6	2.0 ± 0.3	2.3 ± 0.5
W(111)	4.0 ± 0.7	3.1 ± 0.4	5.5 ± 1.6
Polycrystalline W	Not measured	5.5 ± 1.4	6.9 ± 2.1

2.2. Nanoindentation

Nanoindentation testing of the tungsten samples was performed with a commercial nanomechanical test instrument (NanoTest Platform 3, Micro Materials Ltd., Wrexham, UK) which had been calibrated in accordance with the ISO 14577-4. The polycrystalline W was used to determine the frame compliance of the instrument which was confirmed by measurements in other reference metallic samples. The end radii of the diamond indenters were calibrated by fully elastic nanoindentation measurements into fused silica and sapphire reference samples. Three of the indenters used were Berkovich indenters of different end radius and one was spheroconical diamond with a nominalend radius of 5 μm. The fused silica was a nanoindentation intercomparison reference sample (obtained from KRISS, Korea) with a nominal elastic modulus of 72.5 GPa and Poisson's ratio of 0.17. Its elastic properties were separately cross-checked against those of a certified sample (JGC-105, NPL DataSure-IIT reference block) and were found to be consistent to well within 0.5 %. The sapphire was a single crystal with (001) orientation (an intercomparison reference sample from the EU "Nanoindent" project supplied by Roditi, UK). The end radii were 150, 350, 720 and 2800 nm.

The loading conditions for the four indenters are summarised in Table 2.

Table 2. Nanoindentation test conditions

	Loading rate (μN/s)	Peak load (μN)	Hold at peak load (s)	Unloading rate (μN/s)
R = 150 nm	25, 100	500	3	50
R = 350 nm	25, 50, 100, 200	500	3	50
R = 720 nm	25, 100	1000	3	333
R = 2800 nm	100	3000	3	333

Adjacent indentations were made sufficiently far apart (30 μm) to avoid influence from interaction of indentations. The mean values of the critical load, depth, mean pressure and maximum shear stress at pop-in together with their standard deviations for each of the indenters are summarised in Table 3 (a-d). The mean values shown in Table 3 were derived from 35-50 indents for each sample/loading rate/indenter combination with the three sub-micron radius indenters and from 20 indents for R = 2800 μm.

Table 3(a). Pop-in behaviour with the 150 nm end radius indenter

	Critical load (μN)	Depth at pop-in (nm)	Mean pressure at pop-in (GPa)	Maximum shear stress at pop-in (GPa)
W(100) at 25 μN/s	153 ± 99	9.2 ± 3.8	33.7 ± 6.7	15.4 ± 3.1
W(100) at 100 μN/s	124 ± 85	7.2 ± 3.0	32.2 ± 6.6	14.4 ± 2.8
W(111) at 25 μN/s	36 ± 13	3.1 ± 0.9	24.8 ± 3.4	9.8 ± 1.1
W(111) at 100 μN/s	37 ± 13	3.4 ± 0.8	23.2 ± 2.9	9.9 ± 3.5

Table 3(b). Pop-in behaviour with the 350 nm end radius indenter

	Critical load (μN)	Depth at pop-in (nm)	Mean pressure at pop-in (GPa)	Maximum shear stress at pop-in (GPa)
W(100) at 25 μN/s	182 ± 91	7.8 ± 2.8	20.3 ± 3.3	9.4 ± 1.5
W(100) at 100 μN/s	173 ± 102	7.1 ± 3.0	21.1 ± 3.6	9.2 ± 1.7
W(111) at 25 μN/s	69 ± 60	4.3 ± 2.3	13.3 ± 2.6	6.7 ± 1.4
W(111) at 100 μN/s	67 ± 29	4.3 ± 1.3	16.2 ± 1.3	6.8 ± 0.7
Polycrystalline W at 25 μN/s	74 ± 62	4.3 ± 3.0	14.7 ± 2.1	6.7 ± 1.8
Polycrystalline W at 100 μN/s	97 ± 49	5.5 ± 2.4	18.7 ± 1.7	7.6 ± 1.3

Table 3(c). Pop-in behaviour with the 720 nm end radius indenter

	Critical load (μN)	Depth at pop-in (nm)	Mean pressure at pop-in (GPa)	Maximum shear stress at pop-in (GPa)
W(100) at 25 μN/s	226 ± 91	6.8 ± 2.0	14.3 ± 2.8	6.3 ± 1.1
W(100) at 100 μN/s	237 ± 89	6.5 ± 1.8	15.8 ± 2.2	6.4 ± 0.8
W(111) at 25 μN/s	97 ± 95	4.2 ± 3.1	8.5 ± 2.8	4.3 ± 1.6
W(111) at 100 μN/s	100 ± 51	4.2 ± 1.5	10.2 ± 1.6	4.8 ± 0.8

Table 3(d). Pop-in behaviour with the 2800 nm end radius indenter

	Critical load (μN)	Depth at pop-in (nm)	Mean pressure at pop-in (GPa)	Maximum shear stress at pop-in (GPa)
W(100)	380 ± 134	7.3 ± 1.7	5.7 ± 0.8	3.0 ± 0.4
W(111)	250 ± 137	5.3 ± 2.0	5.0 ± 1.2	2.6 ± 0.5

Measurements were also performed with the indenter with end radius R = 350 nm over the load range 10-500 mN where it has the Berkovich geometry. The loading rate was 10 mN/s, the unloading rate was 20 mN/s and the hold at peak load was for 30s. Additional tests were run with a loading time constant equal to 15 s and unloading equal to 2 s. No evidence of rate sensitivity after the 30 s hold at peak load was found, which is consistent with the small indentation creep strain of tungsten at room temperature reported in the past [4]. The thermal drift correction was from 40 s in contact prior to loading and at 90% unloading in all the tests. The reduced indentation modulus (E_r) is related to the elastic modulus (E_s) of the material according to $\frac{1}{E_r} = \frac{1-\upsilon_s^2}{E_s} + \frac{1-\upsilon_i^2}{E_i}$ where E_i is the elastic modulus of the diamond indenter and υ_s and υ_i are the Poisson's ratios of the sample and indenter respectively. For tungsten, a reduced indentation modulus of 321 GPa corresponds to an elastic modulus of 411 GPa. The mean contact pressure up to pop-in can be determined from Hertzian mechanics as $P_m = L/\pi a^2$ where L is the applied load and the contact radius a is given by $a = \sqrt{2Rh_c - h_c^2}$ where $h_c = (h_{max} + h_r)/2$ so that h_c is the contact depth, h_{max} is the depth under load at pop-in and h_r is the residual depth which is taken as zero as the contact is fully elastic to the points considered. The maximum shear stress (τ_{max}) can also be determined from Hertzian analysis. At pop-in, $\tau_{max} = 0.31p_0$ where $p_0 = \sqrt[3]{\frac{6PE_r^2}{\pi^3 R^2}}$.

3. Results

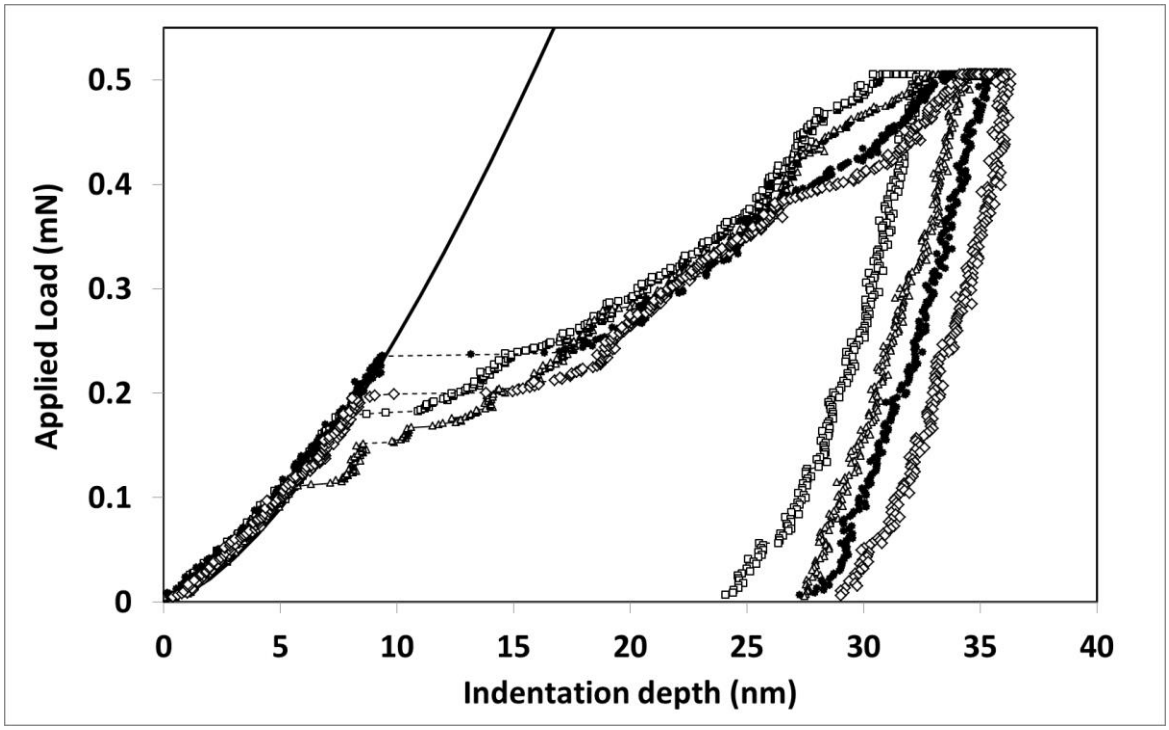

Figure 1: Typical indentation behaviour on the W(100) with the R = 350 nm tip

Typical indentation behaviour on the W(100) with the R = 350 nm probe is shown in figure 1. The loading behaviour is elastic up until a pop-in occurs. If no pop-in occurred before the peak load was reached, then the contact was completely elastic and the entire loading curve could be fitted by Hertzian mechanics (the dotted line in figure 1) using the power-law relationship $P \alpha h^{1.5}$ according to $P = \frac{4}{3} E_r R^{0.5} h^{1.5}$. The pop-in data with the R = 350 nm probe at 100 μN/s are displayed as cumulative probability plots in figures 2(a) to 2(d).

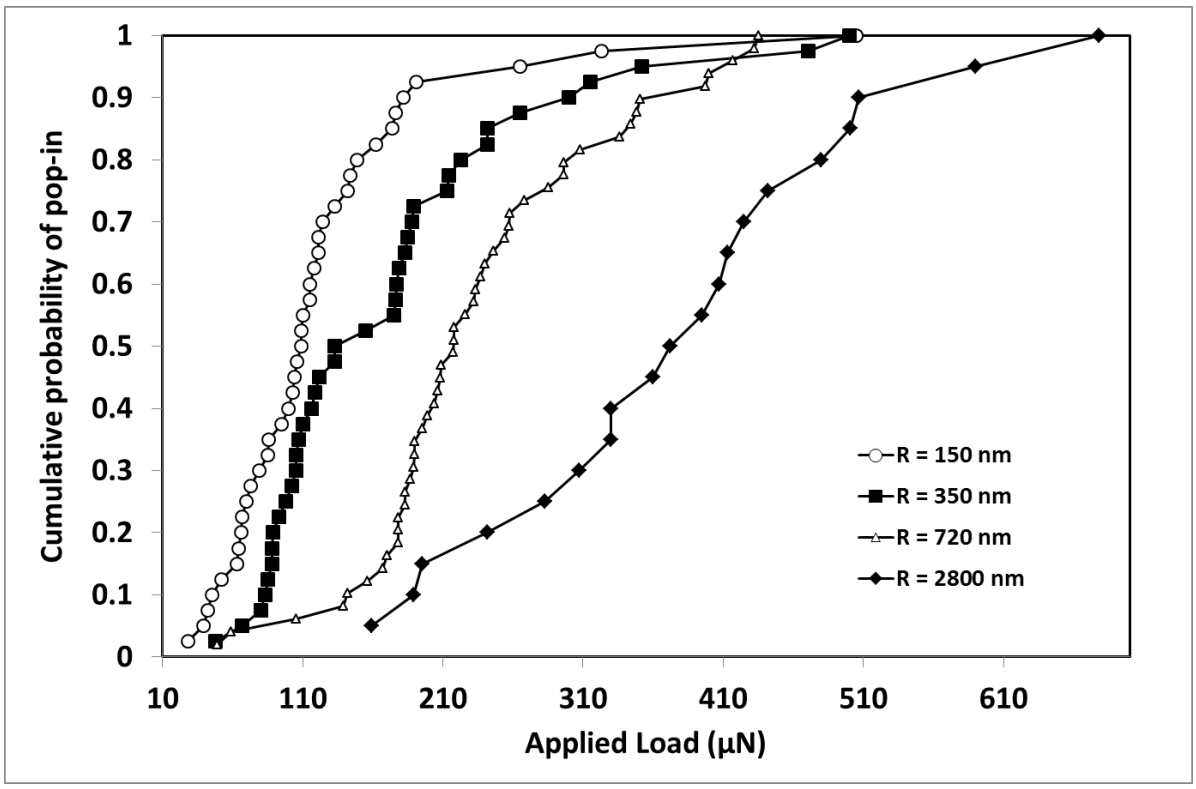

Figure 2(a)

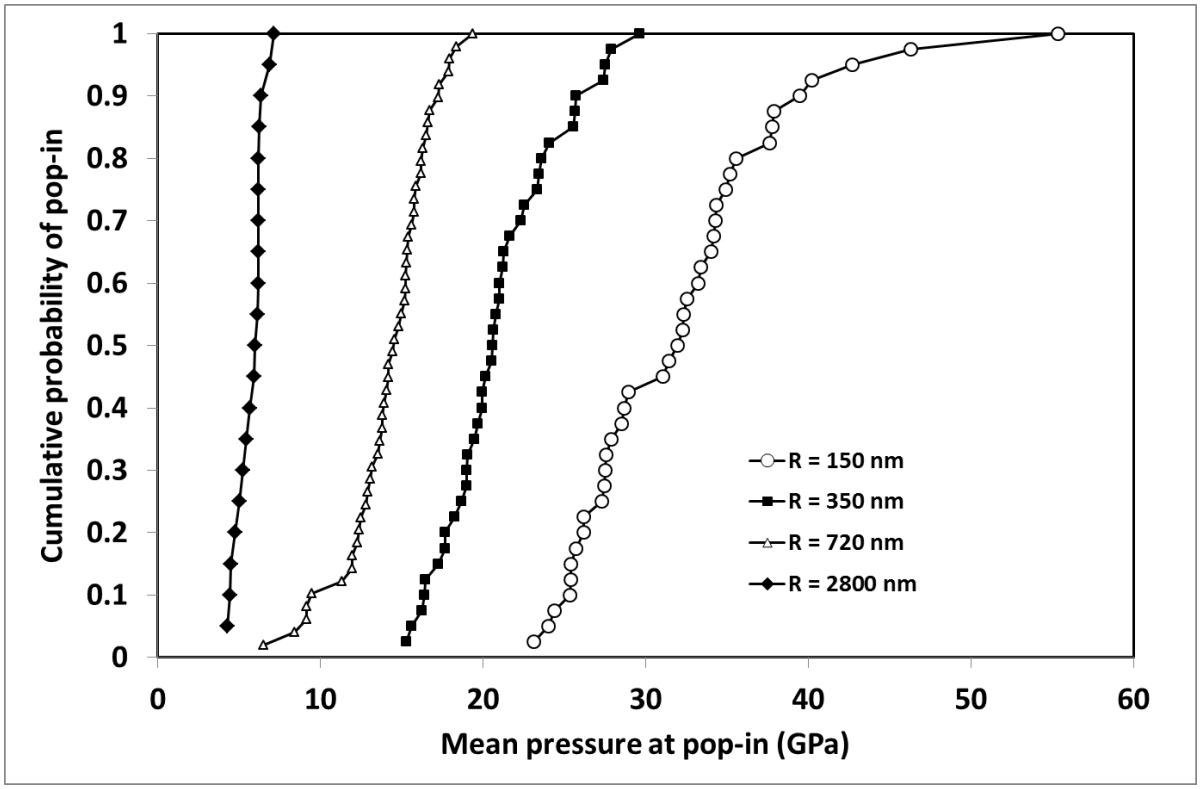

Figure 2(b)

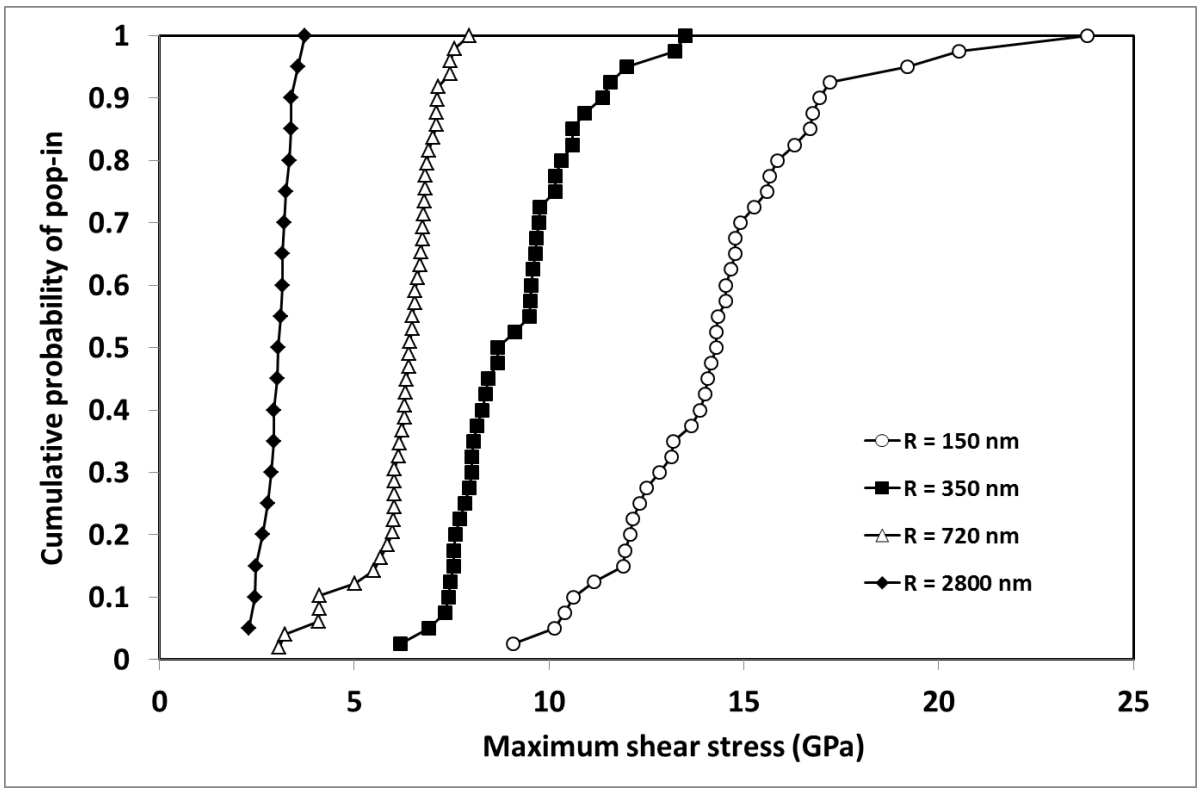

Figure 2(c)

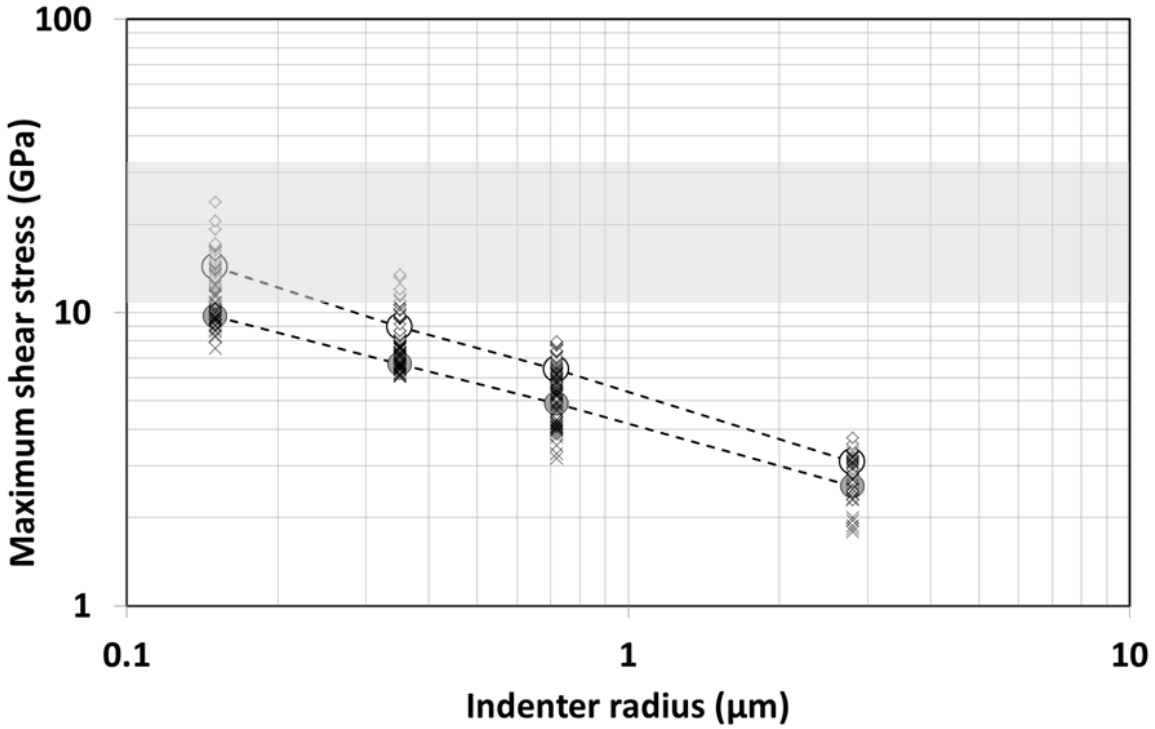

Figure 2(d)

Figure 2: Indenter radius dependence of the pop-in behaviour with loading rate = 100 μN/s (a) critical load (b) mean pressure at pop-in (c) maximum shear stress (d) variation in maximum shear stress with indenter radius for W(100) (diamonds) and W(111) (crosses). The median values at each *R* are shown by the larger circles. The shaded region covers from *G*/5 to *G*/30 where *G* is shear modulus.

The critical load for pop-in on W(100) varied with the indenter radius as shown in Figure 2(a). From Figure 2 in conjunction with Table 3, no evidence was found that would suggest the influence of loading rate on the load required for pop-in on any of the samples studied. The pop-in events were much less pronounced on the W(111) and polycrystalline tungsten samples, with the yield event being more commonly associated with a smaller displacement burst followed by further small periodic events as the load increased. The distribution of cumulative probability of pop-in for W(111) in tests at 25 μN/s or 100 μN/s was different to that for the other two samples as illustrated in Figure 3 for tests at 25 μN/s.

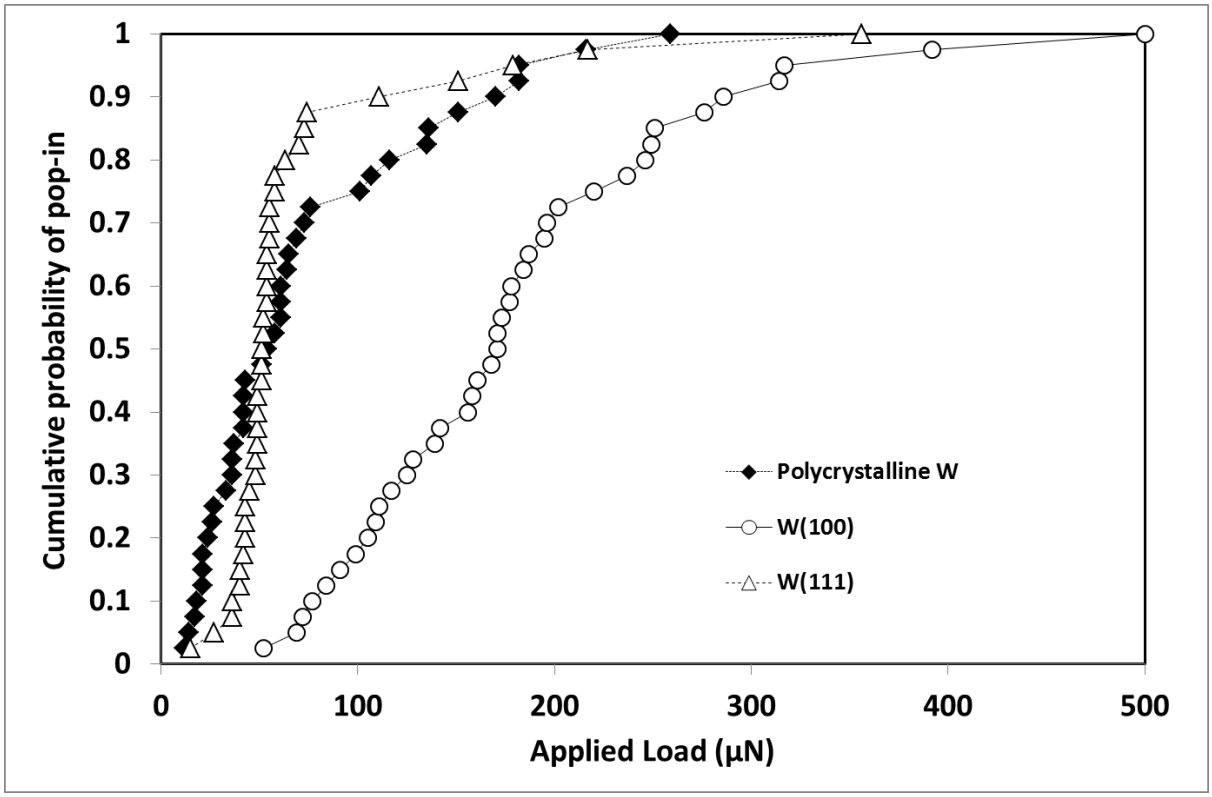

Figure 3: Cumulative probability plots of the critical load on W(100), W(111) and thepolycrystalline W samples with the R = 350 nm tip at 25 μN/s.

The sample with the (111) orientation showed a tighter distribution. After pop-in, the hardness from the unloading curve analysis was lower than the mean pressure in the contact area at pop-in. Analysis of post-yield unloading curves showed the W(111) and polycrystalline tungsten samples to have consistently higher hardness than the W(100) as summarised in Table 4 (a-d).

Table 4(a).Hardness and elastic modulus from nanoindentation to 500 μN with the 150 nm end radius indenter

	H (GPa)	E_r(GPa)	h_c (nm)
W(100) at 25 μN/s	5.45 ± 0.25	322 ± 36	45.9 ± 1.4
W(100) at 100 μN/s	5.99 ± 0.35	322 ± 41	43.2 ± 1.6
W(111) at 25 μN/s	7.84 ± 0.72	345 ± 43	36.3 ± 2.2
W(111) at 100 μN/s	7.52 ± 0.55	320 ± 36	37.2 ± 1.8

Table 4(b).Hardness and elastic modulus from nanoindentation to 500 μN with the 350 nm end radius indenter

	H (GPa)	E_r(GPa)	h_c (nm)
W(100) at 25 μN/s	6.91 ± 0.34	325 ± 39	31.0 ± 1.2
W(100) at 100 μN/s	6.91 ± 0.41	321 ± 43	31.1 ± 1.4
W(111) at 25 μN/s	8.73 ± 1.1	335 ± 47	26.1 ± 2.4
W(111) at 100 μN/s	8.68 ± 0.86	323 ± 41	26.2 ± 1.9
Polycrystalline W at 25 μN/s	9.63 ± 1.1	344 ± 45	24.2 ± 2.0
Polycrystalline W at 100 μN/s	9.43 ± 0.96	338 ± 37	24.5 ± 1.9

Table 4(c).Hardness and elastic modulus from nanoindentation to 1000 μN with the 720 nm end radius indenter

	H (GPa)	E_r (GPa)	h_c (nm)
W(100) at 25 μN/s	5.98 ± 0.25	326 ± 24	40.6 ± 1.4
W(100) at 100 μN/s	6.21 ± 0.27	319 ± 18	41.8 ± 1.4
W(111) at 25 μN/s	7.28 ± 0.68	324 ± 21	35.9 ± 2.6
W(111) at 100 μN/s	7.45 ± 0.55	324 ± 21	35.1 ± 2.0

Table 4(d).Hardness and elastic modulus from nanoindentationto 3000 μN with the2800 nm end radius indenter

	H (GPa)	E_r(GPa)	h_c (nm)
W(100)	4.84 ± 0.20	297 ± 24	35.6 ± 1.5
W(111)	5.84 ± 0.67	301 ± 39	29.8 ± 3.2

The elastic moduli of all three samples were very similar, with the polycrystalline sample being typically ~3 % stiffer. The measurements at higher load confirmed the expected ISE upon hardness for all three samples but not depth dependence of their elastic properties. There was a linear relationship between H^2 and $1/h$ over the depth range of the 10-500 mN data so they were analysed with a Nix-Gao [18] plot using the formula $\frac{H}{H_0} = \sqrt[2]{1 + \frac{h^*}{h}}$ to determine the characteristic length h^* and macroscopic hardness, H_0, which are shown in Table 5.

Table 5.Nix-Gao fitting parameters

	H_0 (GPa)	h^* (nm)
W(100)	3.87	342
W(111)	4.79	463
Polycrystalline W	5.21	278

4. Discussion

Marked crystallographic and contact size effects on the incipient plasticity of tungsten were found in this study. Surface profilometry measurements and indentations to higher loads were used to provide relevant information regarding the surface roughness and conventional size effect upon hardness of the samples. Across the entire load range of the instrument used (0-500 mN), the unloading curve data showed constant elastic modulus, consistent with the literature value (E_r = 321 GPa; E = 411 GPa) with the surface roughness increasing the variability at low indentation depth. Pile-up around the indentation due to cross-slip can increase the contact area leading to an over-estimate of the elastic modulus [19] with an increase of >10% reported for W(100) [20] and ion-irradiated polycrystalline tungsten [21]. In the current study, a much smaller effect was found in line with other recent results on polycrystalline tungsten [21]. The slightly lower modulus obtained from the measurements with the largest radius may also be an effect of the surface roughness together with a reduction in pile-up. Walter et al. [22] reported that the modulus of CrN films with R_a = 2-10 nm was under-estimated by 5-14 % in simulations with a spherical indenter having an end radius of 50μm.

All three samples showed a strong ISE upon hardness with the Nix-Gao plot revealing marked differences in their characteristic length and macroscopic hardness thereby implying a higher dislocation density at or near the surface of the W(111) sample. The rough surface model of Kim et al. [23] suggests that the characteristic length can be under-estimated in the standard Nix-Gao treatment unless roughness is taken into account. For the Ni surfaces, they tested and found that the under-estimations were around 70 nm for surfaces with R_a= 3.2 and 8.7 nm. If similar behaviour of tungsten samples used in this study is assumed, the characteristic length of the polycrystalline sample becomes very close to that of W(100), but its difference with that of W(111)

is increased.

Significantly higher critical loads for pop-in were found for W(100) than for W(111), consistent with previous observations by Yao et al [1]. With an indenter of R = 675 nm, Yao et al [1] reported critical loads on electropolished W single-crystals of the order of 7 mN and 2.5 mN for W(100) and W(111) respectively, corresponding to median shear stresses at pop-in of around 21 and 14 GPa. On Ta, the increase in pop-in load on (100) compared to (110) and (111) has been ascribed to differences in the stresses. FEA analysis showed that the high hydrostatic pressures in the nanoindentation test aid nucleating defects (e.g. twins, stacking faults) [24], with more recent support shown by MD simulations [25].

For W(100), the mean maximum shear stress determined with the R = 150 nm indenter was around 15 GPa, with a maximum value of 23.8 GPa. The theoretical shear strength of crystalline metals can be estimated by dividing the shear modulus by 2π, and is generally quoted to be in the range of $G/5$ to $G/15$. As the shear modulus (G) of W is 161 GPa, the theoretical strength will be in the range of 10.7 to 32.2 GPa, and is 25.6 GPa at $G/2\pi$. The limits at $G/5$ and $G/15$ are shown by the shaded region in Figure 2(d). The data from use of the sharper indenters is consistent with the pop-in occurring when the τ_{max} under the indenter approaches the theoretical strength, as has been reported in previous studies on BCC[9], FCC metals [7] and BCC high-entropy alloys [10]. As shown in Figure 2(d), values of τ_{max} were lower for the (111) orientation of W. Hertzian contact mechanics assumes an ideally flat surface which is however not a practical reality. Although all the tungsten samples were highly polished, Table 1 shows there were differences in surface roughness with the W(111) and polycrystalline W being rougher than the W(100). With an increase in surface roughness, the pressure on the surface of the asperities will be higher than that predicted by the Hertzian treatment (which assumes an initially flat surface) so that although the apparent pressure at pop-in is lower for rougher surfaces the real pressure may be significantly higher, as has been shown in MD simulations of thin copper coatings [26].

In tests on annealed and electropolished tungsten with spherical diamonds with end radii of

1 and 13.5 μm, Pathak et al. [12, 14] observed higher stresses at pop-in with the sharper probe. Data with the blunter probe was more stochastic in nature. Notwithstanding the fact that they tested an electropolished surface, their data was in quite good agreement with the results for W(100) shown in Figure 2 (b). Shim et al [13] provided a qualitative explanation for the radius dependence they found in Ni(100) based on the average dislocation spacing and the stresses required to activate existing dislocations (low stress) or to nucleate new ones in dislocation-free regions (higher stress). Changing the indenter size changed the size of the highly stressed zone (which has been estimated as ~2.4a by Pathak et al. [12, 14]) relative to the average dislocation spacing. If the radius of the indenter tip is much smaller than the spacing needed between dislocations for plasticity to occur, then the applied stress needs to be sufficiently large to nucleate a dislocation. With larger tip radii, the size of the indenter is much larger than the spacing between the dislocation and the stress required to move pre-existing dislocations is lower. Wu et al. [17] recently developed a combined statistical model for the radius dependence providing further evidence that incipient plasticity could be triggered either by homogeneous nucleation of dislocations when a sharp indenter is used or by the activation of existing dislocations when indenting with tips with larger end radii. The strength drops more rapidly with increasing R due to the increasing possibility of encountering pre-existing defects. The model does not consider surface roughness and it seems likely that this will also contribute to the observed size effect. Knap and Ortiz used multiscale simulations to investigate tip-radius effects during nanoindentation of Au(001) with 7 and 70 nm indenters [27]. In their simulations, they found that the dislocation activity occurred before any deviation in the force curve was observed. If a similar trend is also found for BCC metals and continues to larger indenter sizes, then the maximum shear stress-radius dependence would be even larger than has been reported in experimental studies to date.

In the experiments on tungsten performed in this work, there was no discernible rate dependence over 25-200 μN/s in either the stochastics of the pop-ins or the mean load value. Although stress-based thermally activated dislocation nucleation is expected to result in the onset of

plasticity increasing with loading rate [28], the effect is slight in BCC metals compared to FCC metals [9]. Biener et al. [9] reported a very small rate dependence on Ta(001) with RMS roughness well under 1 nm, with the median value of the critical load for pop-in increasing by around 12% over a x100 increase in loading rate from 50 μN/s to 5000 μN/s. The absence of rate dependence in this particular study over a much smaller load range appears to be due to a combination of the intrinsic minimal rate sensitivity of tungsten (where creep strain during the 30 s hold period at peak load in the higher load indentation tests is less than 0.015) and the higher surface roughness (presumably local differences in roughness) of the samples.

Surface preparation is important as it influences the dislocation density and roughness of the final surface [29]. Pathak et al. [12, 14] noted that rough mechanical polishing generally leaves a disturbed surface layer with higher dislocation content which can be removed by electropolishing. On another BCC metal, Mo(001), Wang et al. [30] reported that the highest pop-in critical load was observed after electropolishing. Smaller loads were found after colloidal silica polishing, and polishing by alumina produced defects sufficient to fully suppress pop-in. In a study on a FCC metal, Al (111) by Minor et al. [7], the loading data was fitted to a plot of a Hertzian elastic response. Although surface roughness was not mentioned, the presence of roughness could be inferred by deviation of the experimental data from the elastic fitting by up to ~1 nm. Shibutani et al. [8] studied the influence of surface roughness on the pop-ins observed when indenting Al(001) with a tip of ~50 nm end radius, finding much lower critical loads for less highly polished surfaces. In interfacial force microscopy on a passivated gold surface the critical load for pop-in was reported to be 30-45 % lower near a step than in defect-free regions [31]. In a molecular dynamics study of the influence of surface roughness on nanoindentation, it was reported that defects typically initiate at the side of an asperity [26, 32].

The pop-in events were much less pronounced for the W(111) and polycrystalline tungsten samples, with the yield event being more commonly associated with a smaller displacement burst followed by further small periodic events as the load increased. In addition to the roughness effect

described above, this appears to be partially due to higher dislocation density in these samples causing an increase in the hardness. Studies have also shown that higher pre-existing dislocation density lowers the critical load for pop-in. In high-purity aluminium, a reduction in probability of pop-in was observed when dislocation density increased [33]. In MgO indented with a 9.5 μm tip, Montagne *et al.* [29] noted the contact was elastic up to a load of 300 mN when there were no pre-existing dislocations but reduced nearly to zero for a pre-existing density of 1.2 x 10^7 cm^{-2}. There are differences in the distributions of cumulative probability of the critical load for pop-in between the samples (Figure 3). The extent of dispersion in the first critical load on the FCC Al has been reported to widen with a reduction in roughness [8]. Figure 3 shows that similar behaviour can be seen in W(111). While the average surface roughness is higher on the polycrystalline sample, there are smoother regions so that when indentations are made into these regions the data can more closely approach that obtained from the W(100), but if measurements are made in rougher regions the corresponding critical load is much lower. Yao et al. [1] reported a reduction in critical load for pop-in on W after D-implantation and Biener et al [9] reported a complete suppression on Ta(001) after ion energy ion bombardment. In studies such as these, it is not yet clear how much of the reduction in pop-in is due to surface roughening and how much is due to higher pre-existing dislocations in the near-surface layers of the tungsten. While they are to some extent interlinked, further work on ion-irradiated samples may help to more fully deconvolute these effects.

5.Conclusions

The results being reported in this work confirm the statistical nature of incipient plasticity in the nanoindentation response of tungsten over a wide range of conditions. Indenter radius (and therefore contact size), surface roughness and crystallographic orientation were varied during the experiments. The conclusions can be summarised as follows:

1. A strong size effect was observed, with the stress for incipient plasticity increasing as the indenter radius was decreased. The maximum shear stress approached the theoretical shear

strength when W(100) was indented with the tip with smallest radius, whereas the (111) orientation showed pop-ins at lower stress levels, which has been attributed to surface roughness and greater dislocation density on the W(111) sample

2. Surface preparation plays an important role in the statistical nature of pop-in during loading in nanoindentation tests. While they are to some extent interlinked, it was not clear whether the roughening of the surface itself or the defect generation in the near surface layers caused by it has the greater effect in reducing the load at which pop-in occurs.

Acknowledgments:

Jan Tomastik (Joint Laboratory of Optics, Palacky University and Institute of Physics, Academy of Sciences of the Czech Republic, Olomouc, Czech Republic) is thanked for his assistance with the Nix-Gao analysis of the higher load indentations. SG would like to acknowledge the financial support from the COST Action CA15102 funded by H2020.

References:

[1] W. Yao, P. Wang, A. Manhard, C. Krill III, J. You, Effect of hydrogen on the slip resistance of tungsten single crystals, Materials Science and Engineering: A 559 (2013) 467-473.
[2] J.S.-L. Gibson, S.G. Roberts, D.E. Armstrong, High temperature indentation of helium-implanted tungsten, Materials Science and Engineering: A 625 (2015) 380-384.
[3] R. Abernethy, Predicting the performance of tungsten in a fusion environment: a literature review, Mater Sci Tech-Lond 33(4) (2017) 388-399.
[4] A.J. Harris, B.D. Beake, D.E. Armstrong, M.I. Davies, Development of high temperature nanoindentation methodology and its application in the nanoindentation of polycrystalline tungsten in vacuum to 950 C, Experimental Mechanics 57(7) (2017) 1115-1126.
[5] S. Goel, G. Cross, A. Stukowski, E. Gamsjäger, B.D. Beake, A. Agrawal, Designing nanoindentation simulation studies by appropriate indenter choices: Case study on single crystal tungsten (under review), Comp Mater Sci (2018).
[6] D.F. Bahr, D.E. Kramer, W.W. Gerberich, Non-linear deformation mechanisms during nanoindentation, Acta Mater 46(10) (1998) 3605-3617.
[7] A. Minor, E. Lilleodden, E. Stach, J. Morris, Direct observations of incipient plasticity during nanoindentation of Al, J Mater Res 19(1) (2004) 176-182.
[8] Y. Shibutani, A. Koyama, Surface roughness effects on the displacement bursts observed in nanoindentation, J Mater Res 19(1) (2004) 183-188.
[9] M.M. Biener, J. Biener, A.M. Hodge, A.V. Hamza, Dislocation nucleation in bcc Ta single crystals studied by nanoindentation, Phys Rev B 76(16) (2007) 165422.
[10] Y. Ye, Z. Lu, T. Nieh, Dislocation nucleation during nanoindentation in a body-centered cubic

TiZrHfNb high-entropy alloy, Scripta Mater 130 (2017) 64-68.
[11] C. Wilson, J. McCormick, A. Cavanagh, D. Goldstein, A. Weimer, S. George, Tungsten atomic layer deposition on polymers, Thin Solid Films 516(18) (2008) 6175-6185.
[12] S. Pathak, D. Stojakovic, R. Doherty, S.R. Kalidindi, Importance of surface preparation on the nano-indentation stress-strain curves measured in metals, J Mater Res 24(3) (2009) 1142-1155.
[13] S. Shim, H. Bei, E.P. George, G.M. Pharr, A different type of indentation size effect, Scripta Mater 59(10) (2008) 1095-1098.
[14] S. Pathak, S.R. Kalidindi, Spherical nanoindentation stress–strain curves, Materials Science and Engineering: R: Reports 91 (2015) 1-36.
[15] N. Stelmashenko, M. Walls, L. Brown, Y.V. Milman, Microindentations on W and Mo oriented single crystals: an STM study, Acta Metall Mater 41(10) (1993) 2855-2865.
[16] S. Syed Asif, J. Pethica, Nanoindentation creep of single-crystal tungsten and gallium arsenide, Philosophical Magazine A 76(6) (1997) 1105-1118.
[17] D. Wu, J.R. Morris, T. Nieh, Effect of tip radius on the incipient plasticity of chromium studied by nanoindentation, Scripta Mater 94 (2015) 52-55.
[18] W.D. Nix, H. Gao, Indentation size effects in crystalline materials: a law for strain gradient plasticity, J Mech Phys Solids 46(3) (1998) 411-425.
[19] N. Moharrami, S. Bull, A comparison of nanoindentation pile-up in bulk materials and thin films, Thin Solid Films 572 (2014) 189-199.
[20] Y.-H. Lee, U. Baek, Y.-I. Kim, S.-H. Nahm, On the measurement of pile-up corrected hardness based on the early Hertzian loading analysis, Mater Lett 61(19-20) (2007) 4039-4042.
[21] C.E. Beck, F. Hofmann, J.K. Eliason, A.A. Maznev, K.A. Nelson, D.E. Armstrong, Correcting for contact area changes in nanoindentation using surface acoustic waves, Scripta Mater 128 (2017) 83-86.
[22] C. Walter, T. Antretter, R. Daniel, C. Mitterer, Finite element simulation of the effect of surface roughness on nanoindentation of thin films with spherical indenters, Surface and coatings technology 202(4-7) (2007) 1103-1107.
[23] J.-Y. Kim, S.-K. Kang, J.-J. Lee, J.-i. Jang, Y.-H. Lee, D. Kwon, Influence of surface-roughness on indentation size effect, Acta Mater 55(10) (2007) 3555-3562.
[24] O. Franke, J. Alcalá, R. Dalmau, Z.C. Duan, J. Biener, M. Biener, A.M. Hodge, Incipient plasticity of single-crystal tantalum as a function of temperature and orientation, Philos Mag 95(16-18) (2015) 1866-1877.
[25] S. Goel, B.D. Beake, C.-W. Chan, N. Haque Faisal, N. Dunne, Twinning anisotropy of tantalum during nanoindentation, Materials Science and Engineering: A 627(0) (2015) 249-261.
[26] P. Hansson, Influence of surface roughening on indentation behavior of thin copper coatings using a molecular dynamics approach, Comp Mater Sci 117 (2016) 233-239.
[27] J. Knap, M. Ortiz, Effect of indenter-radius size on Au (001) nanoindentation, Phys Rev Lett 90(22) (2003) 226102.
[28] D. Chrobak, K.-H. Kim, K. Kurzydłowski, R. Nowak, Nanoindentation experiments with different loading rate distinguish the mechanism of incipient plasticity, Appl Phys Lett 103(7) (2013) 072101.
[29] A. Montagne, V. Audurier, C. Tromas, Influence of pre-existing dislocations on the pop-in phenomenon during nanoindentation in MgO, Acta Mater 61(13) (2013) 4778-4786.
[30] Z. Wang, H. Bei, E.P. George, G.M. Pharr, Influences of surface preparation on nanoindentation pop-in in single-crystal Mo, Scripta Mater 65(6) (2011) 469-472.
[31] J. Kiely, R. Hwang, J. Houston, Effect of surface steps on the plastic threshold in nanoindentation, Phys Rev Lett 81(20) (1998) 4424.
[32] S. Goel, W.B. Rashid, X. Luo, A. Agrawal, V. Jain, A theoretical assessment of surface defect machining and hot machining of nanocrystalline silicon carbide, Journal of Manufacturing Science and Engineering 136(2) (2014) 021015.
[33] A. Barnoush, Correlation between dislocation density and nanomechanical response during nanoindentation, Acta Mater 60(3) (2012) 1268-1277.